Supporting Information

Xiao et al. 10.1073/pnas.1702405114

Computational Details. The calculations were first performed with the VASP package (34–36), using the Perdew–Burke–Ernzerhof (PBE) flavor (37) of DFT and the projector augmented wave (PAW) method (38) to account for core–valence interactions. The kinetic energy cutoff for plane-wave expansions was set to 400 eV, and reciprocal space was sampled by a Γ-centered Monkhorst–Pack scheme with a grid of $3 \times 3 \times 1$. The 4×4 Cu(111) and 2×2 Cu_2O(111) surface slabs were constructed with three layers (bottom layer fixed), using the experimental lattice parameters of 3.615 Å and 4.2745 Å, respectively, with vacuum layers of at least 15 Å.

The convergence criteria are 1×10^{-5} eV and 1×10^{-7} eV energy differences for solving for the electronic wavefunction for local minima [initial states (ISs) and FSs] and TSs, respectively. The Methfessel–Paxton smearing of second order with a width of 0.1 eV was applied. All IS, TS, and FS geometries (atomic coordinates) are converged to within 3×10^{-2} eV/Å for maximal components of forces. The TS search was conducted by using the climbing-image nudged elastic band (CI-NEB) method (39) to generate initial guess geometries, followed by the dimer method (40) to converge to the saddle points.

Zero-point energy (ZPE), enthalpy, and entropy contributions to free energies at room temperature (298.15 K) were calculated from vibrational modes of surface species, which were computed with the finite difference approach. Note that very low-frequency modes were obtained in some cases, because the explicit water molecules are not properly constrained by the hydrogen-bonding network present in water bulk. Such low-frequency modes can cause unphysically large entropy contributions, so they were reset to a threshold value of 60 cm^{-1}, corresponding to the acoustic translational mode of the six-member rings in water bulk (41, 42).

For the CO hydrogenation step where the surface H model was used to locate the TS, the IS was referenced back to the $H^+(H_3O^+/H_2O) + e^-$ pair through the free energy difference between the surface H and H_2(g), based on the half-cell reactions,

$$H_3O^+ + e^- = \frac{1}{2} H_2(g) + H_2O \quad \Delta G = 0.0592 \times pH\,(eV),$$
$$H_2O + e^- = \frac{1}{2} H_2(g) + OH^- \quad \Delta G = 0.0592 \times pH\,(eV).$$

Thus, the pH effect is introduced into the free energy profile with the reference. In addition to vibrational contributions, the translational and rotational contributions to the free energy of H_2(g) were included, assuming the ideal gas model.

The explicit constant electrochemical potential (μ_e) calculations with the implicit CANDLE solvation model (19) were performed upon all IS, TS, and FS geometries, using JDFTx (43). The Garrity–Bennett–Rabe–Vanderbilt (GBRV) (44) ultrasoft pseudopotentials (USPP) were used, with a plane-wave cutoff of 544 eV (20 a.u.). All other settings are similar to those in VASP calculations. The ionic screening of net charges resulting from the constant μ_e condition was achieved with cation (0.1 M K^+) and anion (0.1 M F^-) components in the fluid model (21) under the JDFT framework (20). The algorithm used by JDFTx variationally minimizes the grand free energy at fixed electron chemical potential with respect to Kohn–Sham orbitals (45), fluid bound charge, and an auxiliary Hamiltonian for the occupations (46). Previously we found that the relative free energies (barriers $\Delta G^{\neq}$ and reaction energies ΔG) are linearly dependent on the applied potential U for $|U| < \sim 2$ V [vs. standard hydrogen electrode (SHE)] (17), so the U dependence of all $\Delta G^{\neq}$ and ΔG was calculated assuming a linear relationship between U = 0.0 V and −1.2 V. Note that here all Us are referenced to SHE.

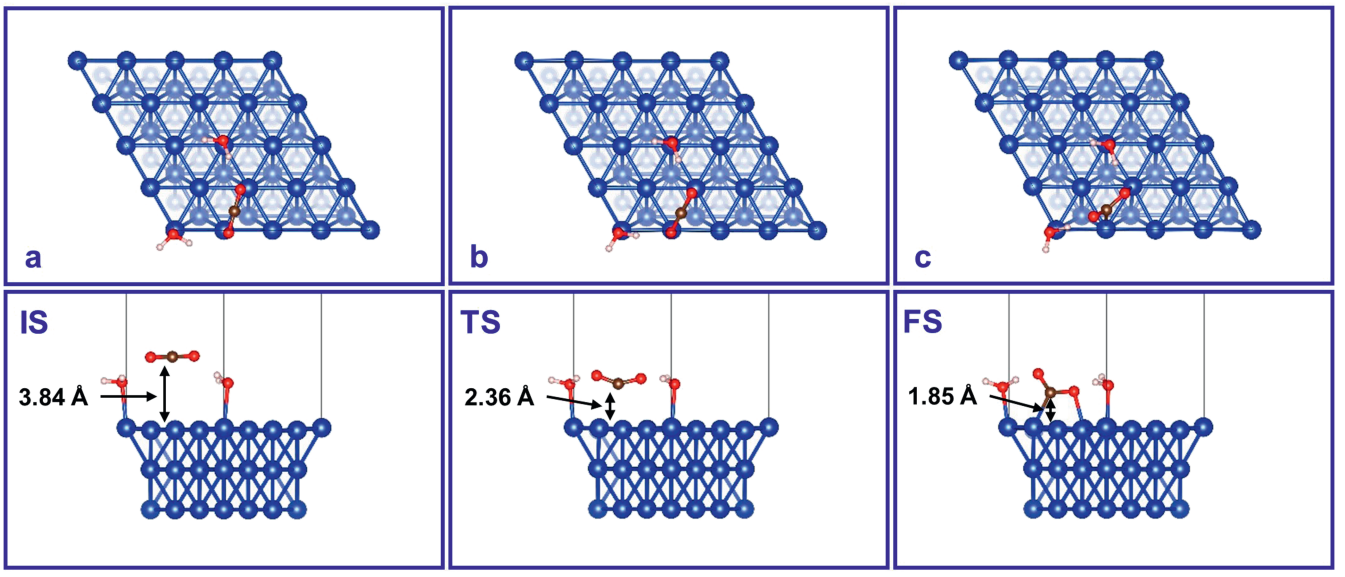

Fig. S1. Top and side views of (*A*) IS, (*B*) TS, and (*C*) FS for the CO_2 activation on Cu MM. The marked distances are between the C atom of CO_2 and the Cu surface. In the FS (chemisorbed CO_2), Cu-C and Cu-O bond lengths are 2.05 Å and 2.04 Å, respectively.

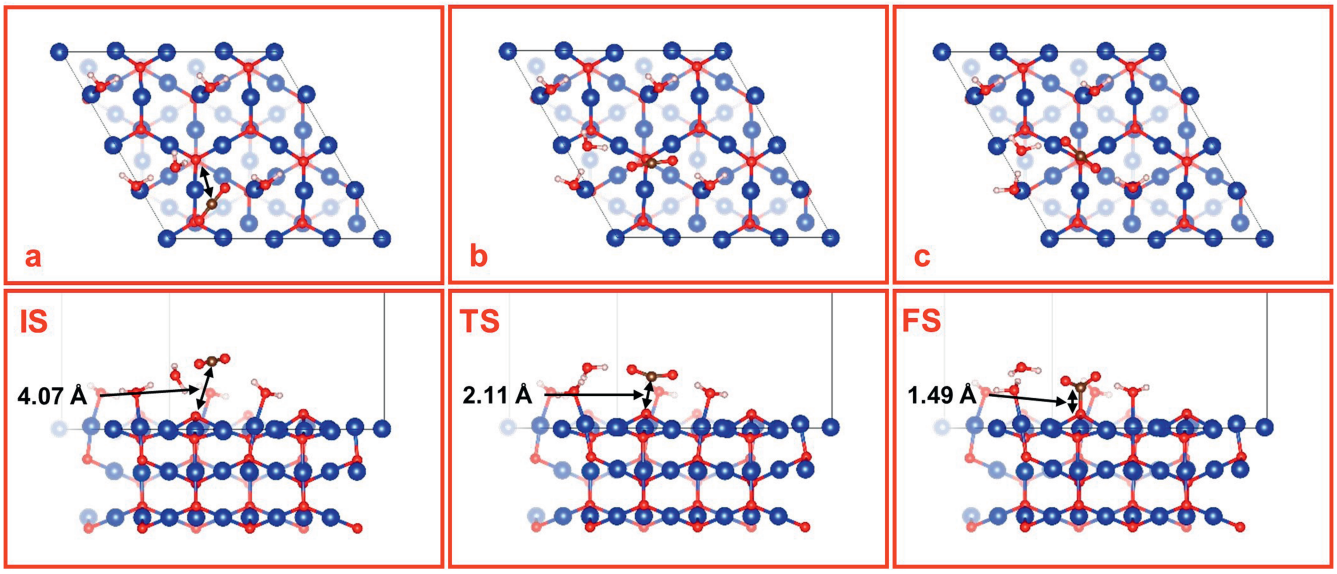

Fig. S2. Top and side views of (*A*) IS, (*B*) TS, and (*C*) FS for the CO_2 activation on FOM. The marked distances are between the C atom of CO_2 and the surface O atom that is bonded to CO_2 in the FS. Note that a surface carbonate is formed in the FS.

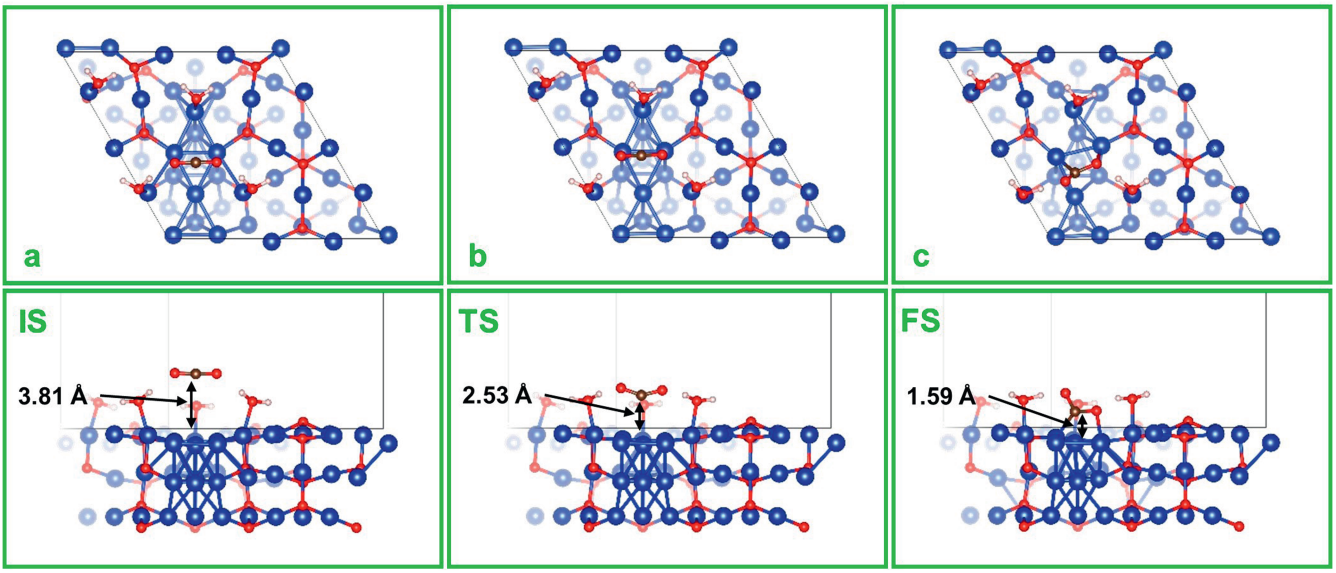

Fig. S3. Top and side views of (*A*) IS, (*B*) TS, and (*C*) FS for the CO_2 activation on MEOM. The marked distances are between the C atom of CO_2 and the Cu metallic region surface. In the FS (chemisorbed CO_2), Cu-C and Cu-O bond lengths are 2.02 Å and 2.04 Å, respectively.

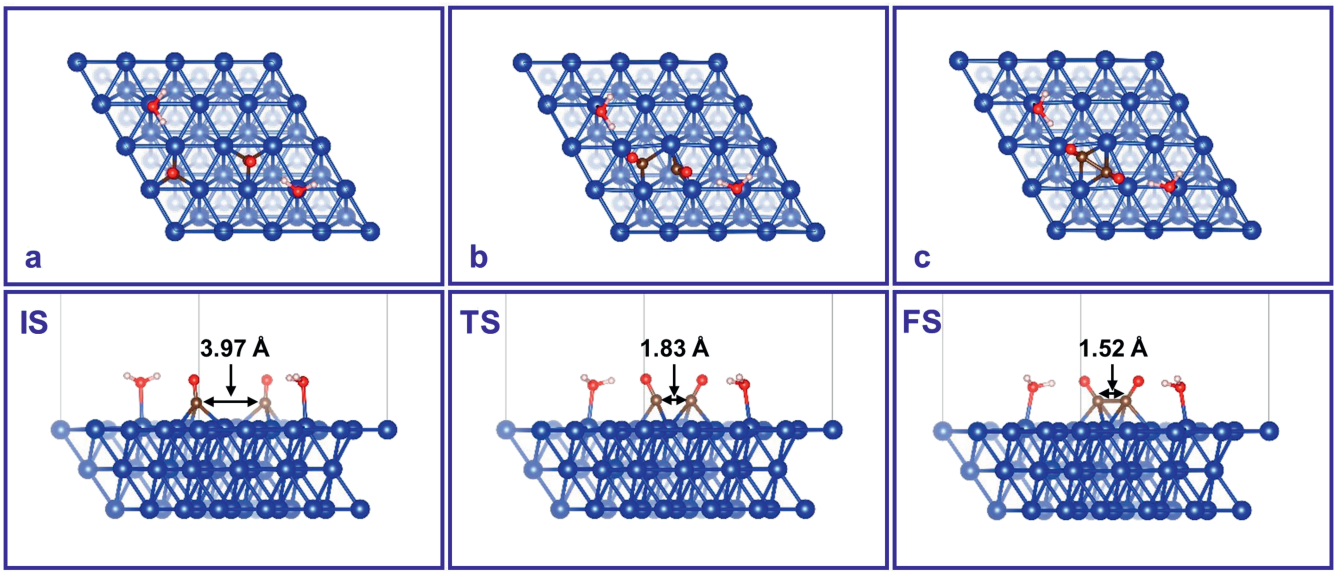

Fig. S4. Top and side views of (*A*) IS, (*B*) TS, and (*C*) FS for the CO dimerization on Cu MM. The marked distances are between the two C atoms of CO.

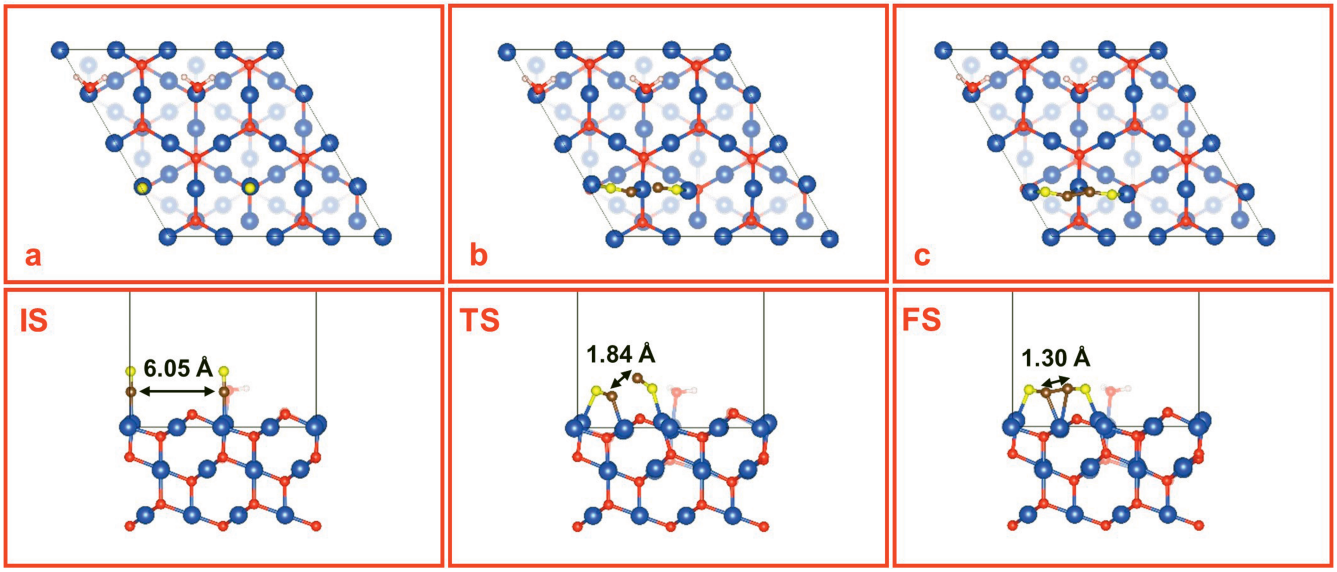

Fig. S5. Top and side views of (*A*) IS, (*B*) TS, and (*C*) FS for the CO dimerization on FOM. The marked distances are between the two C atoms of CO. Note that the O atoms of CO are colored yellow for clarity.

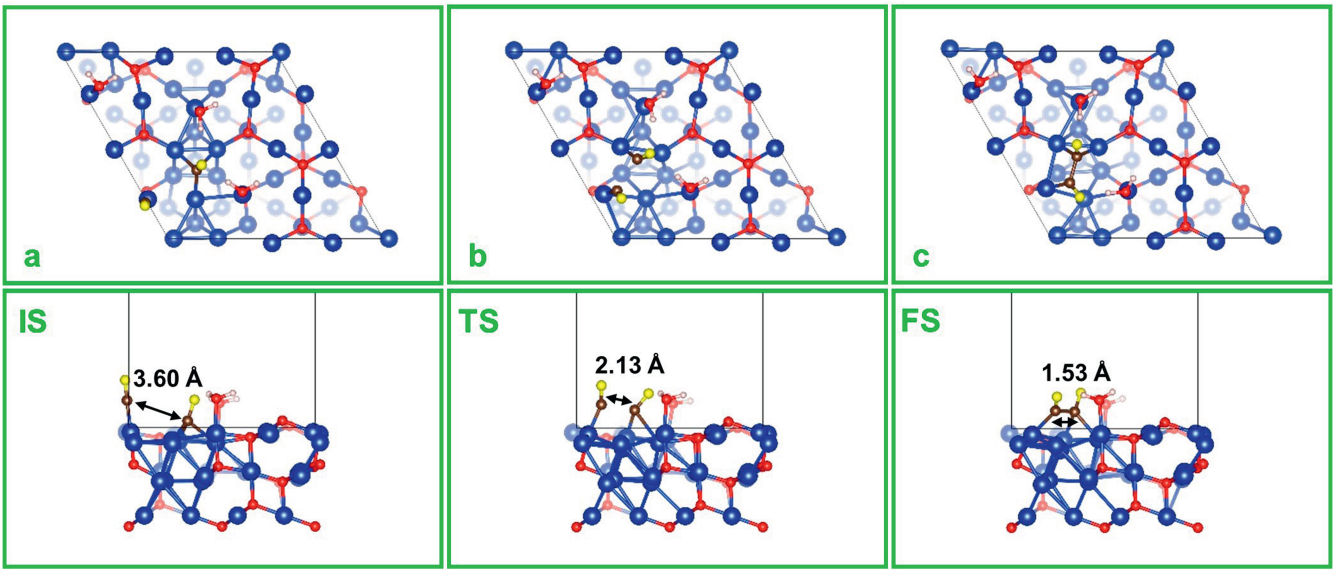

Fig. S6. Top and side views of (*A*) IS, (*B*) TS, and (*C*) FS for the CO dimerization on MEOM. The marked distances are between the two C atoms of CO. Note that the O atoms of CO are colored yellow for clarity.

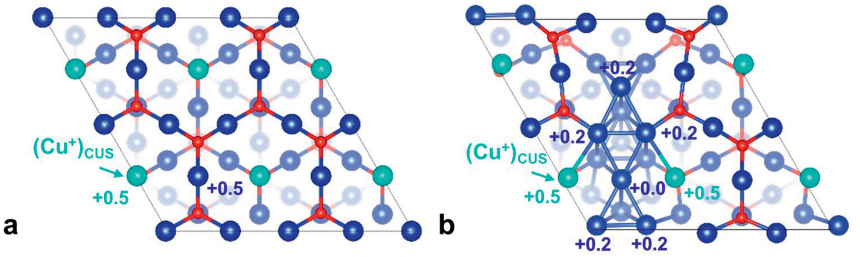

Fig. S7. Bader charges for representative sites on (*A*) FOM and (*B*) MEOM surfaces.

Table S1. Free energy barriers ($\Delta G^{\neq}$) and reaction free energies (ΔG) for all key reactions

Reaction	$\Delta G^{\neq}$, eV	ΔG, eV
CO_2(phys) = CO_2(chem) on M	0.5914 + 0.1117 × U	0.5021 + 0.3356 × U
CO_2(phys) = CO_2(chem) on FOM	0.6140 + 0.0593 × U	0.2508 + 0.1488 × U
CO_2(phys) = CO_2(chem) on MEOM	0.3636 + 0.1077 × U	0.0407 + 0.3392 × U
2CO = OCCO on M	1.1664 + 0.0764 × U	1.0812 + 0.2407 × U
2CO = OCCO on FOM	3.2747 + 0.1383 × U	2.8487 + 0.6696 × U
2CO = OCCO on MEOM	0.8602 + 0.1688 × U	0.4670 + 0.3828 × U